III. Természettudományok

Bolf, Márton

Designing and testing of a microfluidic focuser device

Supervisor: Dr. Laki, András József
(Associate Professor at the Pázmány Péter Catholic University, Faculty of Information Technology and Bionics)

Micorfluidics is an interdisciplinary science field which handles fluid driven systems where macrofluidic laws do not apply. Experiments related to microfluidic devices are more and more widespread in these days since the importance of knowing these systems is the key for modern biochemical and pharmaceutical research. Experiments with microfluidic devices can be conducted within minutes using minimal amount of sample this way it makes measurements cheaper and faster than former approaches. This essay records the fabrication and experimental testing of a microfluidic focuser devise. The emphasis is on the passive microfluidic approach which uses the flow of the fluid to manipulate particles inside the microfluidic channel. The device designed and tested during the measurements is a microfluidic focuser which uses a so called "serpentine" geometry to move the particles to the middle of the channel. During the experiments multiple versions of the device were tested and evaluated to determine the main parameters of the system which influence the focusing performance of the chip.

1. Introduction

Micorfluidics is an interdisciplinary science field which handles fluid driven systems where macrofluidic laws do not apply. One of the main goals of microfluidic experiments is to control particles inside the fluid having different properties (size, weight, elasticity, etc.). The manipulation of these particles can happen in a variety of different ways like using electromagnetic field, light, heat, and any other external source which can be regulated adequately. From the broad variety of possible options this study elaborates on the passive microfluidic approach (Narayanamurthy et al., 2020). In passive microfluidic devices the particles inside the channel are manipulated using solely the driving force of the fluid surrounding them. The flow profile can be adjusted by differently shaped channels each having unique effect on it.

In this report the device has a serpentine region which is responsible for creating the driving force which makes the particles drift to the middle of the channel. This driving force is called Dean flow (Nivedita, Ligrani, & Papautsky, 2017) and is a cross sectional flow which is produced by the curved segments of the channel. This flow creates a pressure gradient along the cross section of the channel which induces a flow which is perpendicular to the flow direction. This pressure gradient makes it possible to use the device as a microfluidic focuser (Martel & Toner, 2014). The utilization of the Dean flow is usually happening in spiral

devices (Xiang et al., 2015; Xiang, Ni, & Yi, 2018). These devices have an inlet in the middle of the chip and two outlets at the end of the spiral. In this report a different type of focuser device is tested which has a serpentine region between the inlet and the outlets.

2. Microfluidic design and fabrication

The microfluidic devices were designed in AutoCAD (*T.53.0.0 AutoCAD 2023, San Rafael (California), United States*) software. For the measurements 100 µm, 150 *µm* and 200 *µm* wide channels were created (annotated as parameter *W* on figures 1 and 2). The length of the parallel segments in the serpentine region (marked as *L* on figure 1) was also adjusted (from 0.5 mm to 2.0 mm using 0.5 mm steps) to see its effect on the focusing ability. This way the experiments are comparable between the different sized channels and the best performing device can be selected (and modified further for better results in the future). The device schematics are presented on figures 1 and 2. The chip has one inlet and three outlets. It has a serpentine section where the focusing of the drifting particles happens (figure 1.). The flow stream is broken by an expanded region (figure 2.) right before the outlets to make the path of the particles observable.

The device was fabricated using PDMS (Polydimethylsiloxane)-glass technique and the master mold was created using laser ablation. The fabrication processes are shown on figure 3. from article (Akther, Yakob, Nguyen, & Ta, 2020). Using this technique, durable and disposable devices can be manufactured.

Figure 1: Schematics of the microfluidic device used for the measurements: Beside the most important parameters and flow direction the winding part of the channel is demonstrated and annotated. The most important part of the device is the serpentine region, which is magnified here. The parameter W stands for the width of the channel while L is the length of the parallel sections in the serpentine region.

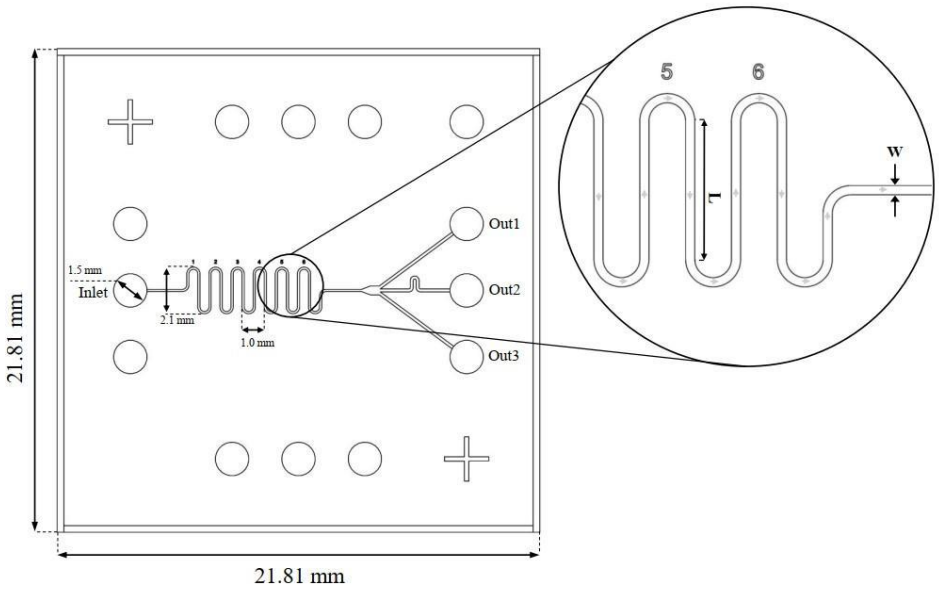

Source: Own work, 2022

Figure 2: Schematics of the microfluidic device used for the measurements: In this figure the expanding region of the device is magnified. W is the width of the channel which was adjusted during the experiments. The expanding region is used for making the path of the particles observable.

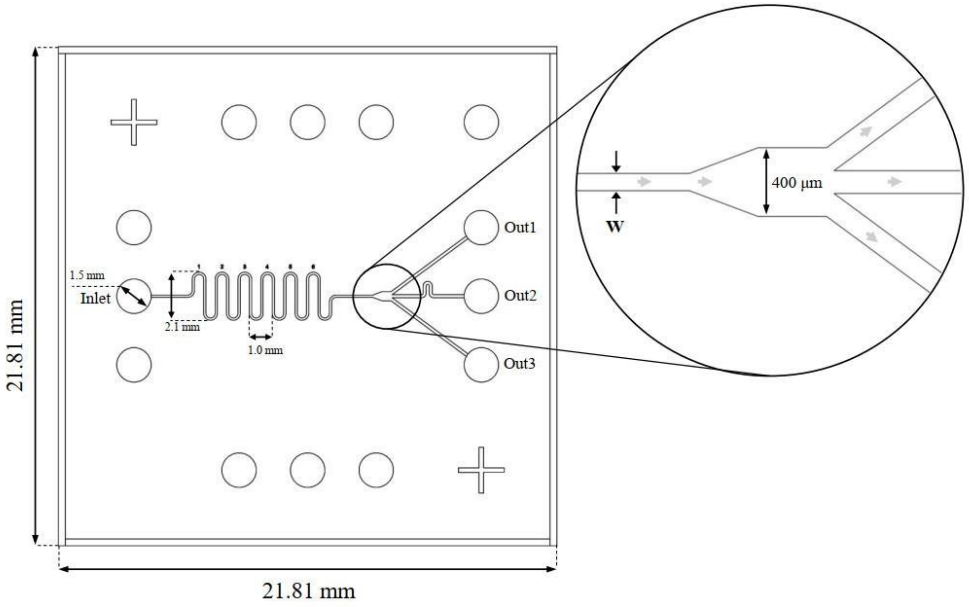

Source: Own work, 2022

Figure 3: Fabrication steps of the PDMS-glass technique: First, the master mold is created using photoresist and laser ablation.(1) After, the PDMS is poured onto the mold and conditioned until it reaches the proper solidity.(2) The PDMS plate gets removed(3) so the inlets and outlets can be drilled and the excess polymer can be removed from them.(4) Finally, the PDMS chip and the glass plate are plasma treated and pressed together forming covalent bond on the contiguous surfaces (5).

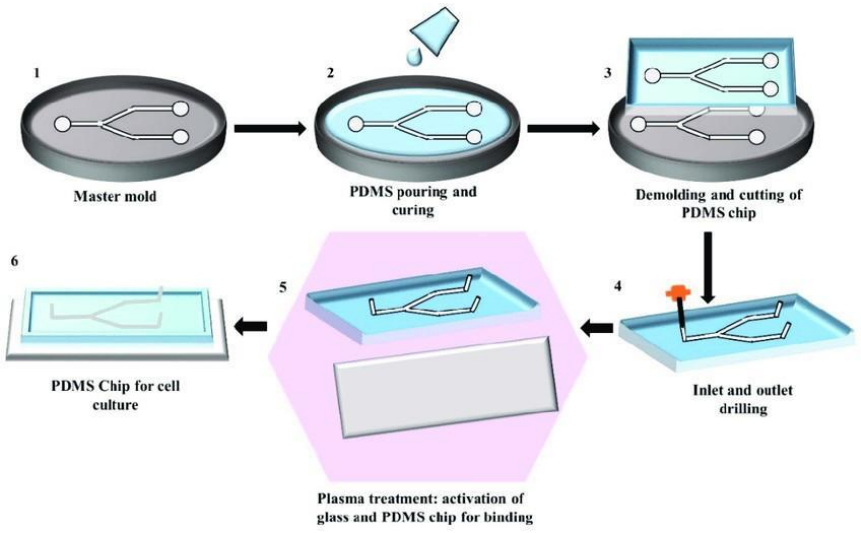

Source: Akther, Yakob, Nguyen, & Ta, 2020

3. Microfluidic platform

Below, the experimental setup is demonstrated, and the different components of the microfluidic platform are discussed.

3.1. Syringe pump

During the experiments a syringe pump was ensuring fixed flow rate along the whole duration of the measurements. The flow rate was set to the maximum value the channel can endure. This means that the devices having bigger channel width were examined under higher flow rates than the thinner variants. The syringe pump used for the experiment was a New Era Pump Systems *(NE-1000, New York, United States)* model ('Syringe Pump - Advanced Precision Programmable Syringe Pumps - SyringePump.com', n.d.).

3.2. Inverted microscope

The results are mostly the outcomes of image analysis. To achieve accurate measurements the usage of a microscope was required. An inverted microscope has bigger working space than a regular one, therefore this type of device was chosen. The microscope used during the experiments was an Olympus *(CKX53, Tokyo, Japan)* model which – thanks to its camera insertion slot – made the recording of the experiments possible ('CKX53 | Compact Cell Culture Microscope | Olympus LS', n.d.).

3.3. Camera

The measurement was recorded using a microscope-compatible IDS camera *(UI-3180CP Rev. 2.1, Obersulm, Germany)* ('UI-3180CP Rev. 2.1', n.d.). The recording properties (frame rate, exposure, bit rate) were adjusted for the type of the measurements (for example timelapse imaging requires low frame rate and higher exposure for better results).

3.4. Measurement layout

The above devices were composing the measurement platform. The experimental setup consists of a syringe pump (which worked as a supplier pressing the microbead solution into the microfluidic device), an inverted microscope and the eppendorf tubes storing the output of the microfluidic device. The device was placed into the inverted microscope to take pictures (using the inserted camera) and examine the device in real time during the measurements. The outlets of the chip were connected with the eppendorf tubes (using teflon tubes), which contained the output liquid for particle counting (using Bürker chamber). The schematics of the measurement setup are shown on figure 4.

Figure 4: The schematics of the measurement arrangement: The chip was placed under an inverted microscope (which made the examination of the transparent device possible). The inflow of the experimental solution was provided by a syringe pump and the effluent samples were stored in eppendorf tubes. For the connections between the syringe and the inlet and between the chip outlets and eppendorf tubes teflon tubing (Masterflex Transfer Tubing, Microbore PTFE, 0.012" ID x 0.030" OD) was used.

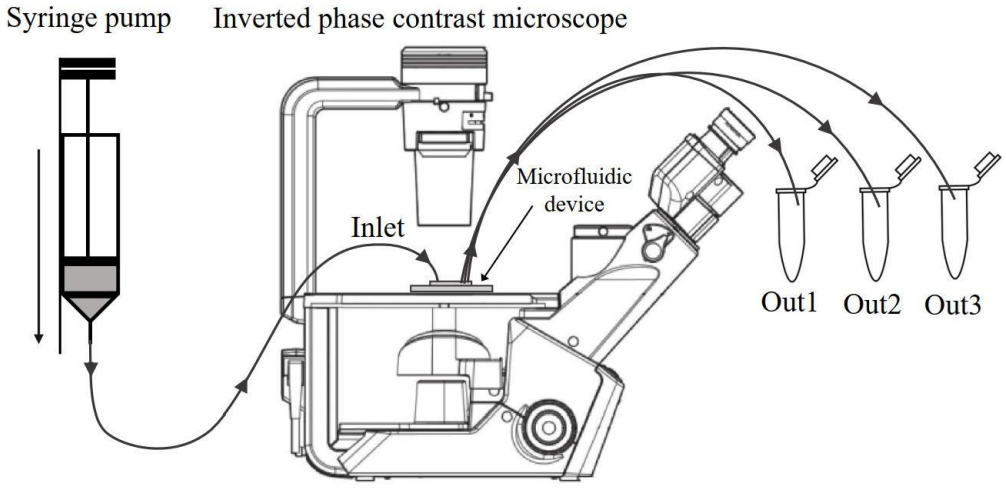

Source: Own work, 2022

4. Materials

In this section the materials used for the measurements are going to be presented.

4.1. Experimental microbead solution

During the measurements the composition of the microbead solution was the same for comparable results. The ingredients (for 1 ml solution) were the following:

- 980 μl Cell Culture Grade Water *(Cytiva, Marlborough, United Kingdom)*
- 10 μl Tween® 20 (1:20 dilution with water) surfactant
- 10 μl Micromer® microbead solution *(Micromod Partikeltechnologie GmbH, Schillingallee, Germany)*; the size of the beads (2 μm, 5 μm, 10 μm) was selected according to the exeriments.

4.2. PDMS

The device was fabricated using PDMS-glass technique (figure 3). PDMS is a polymer, used for fast fabrication processes like the microfluidic device molding. The PDMS solution used for the device fabrication was created using the Sylgard 184 Silicone elastomer kit *(Dow, Midland (Michigan), United States)* ('SYLGARD^{TM} 184 Silicone Elastomer Kit', n.d.).

4.3. Photoresist

Photoresists are special materials capable of changing their state of matter (become fluid from solid or vice versa) when exposed to light. The master mold of the device is created using photoresist coating on a silicon wafer. The details of the device are "burned" in the resist using laser. The excess resist then can be washed away from the wafer only leaving the master mold structure behind. The photoresist used for the fabrication of the microfluidic devices is a Micro Resist Technology coating *(SU8-2000 series, Berlin, Germany)* ('SU-8 2000 series – Microresist', n.d.).

4.4. Silicon Wafer

Silicon wafers were used for creating the master mold of the microfluidic device. It creates a base for photoresist coating. The wafers used in the laboratory for this purpose are Siegert Wafer GmbH fabricated (Si-Wafer 4P0/>1/525±25/SSP/TTV<10, Aachen, Germany) ('Silicon Wafers, Si-Wafers - SIEGERT WAFER GmbH', n.d.).

5. Methods

The following techniques were used for measurements. These approaches mainly rely on image processing and manual counting of the particles using microscope. It is important to note the inaccuracy of these measurements and that the outcomes can vary from experiment to experiment. Even so, these techniques give sufficiently precise results for estimating the main characteristics of the microfluidic devices tested.

5.1. Timelapse imaging

With this technique the frames of a continuous video were stacked on one another. This way the path of microbeads can be displayed on one image as a darker band inside the channel.

5.2. Histogram

Using the frames of the video file mentioned in section 5.1 the exact location of the particles can be measured. During these experiments the location was compared to the upper wall of the extensive region as shown on figure 5.

Figure 5: Interpretation of the histogram data: The intervals shown on the histogram are the distances from the upper wall of the channel and were measured in the cross section shown above as a dashed line. if more particles were counted in one interval the percentage of these regions grow compared to the others.

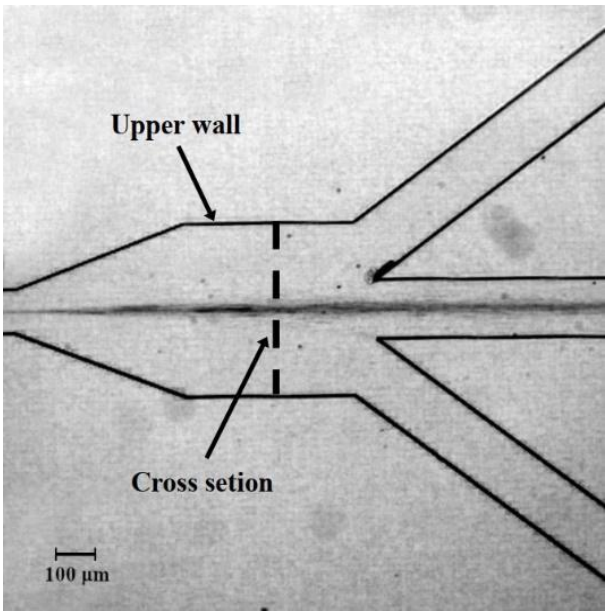

Source: Own work, 2022

5.3. Particle counting using Bürker chamber

The measurements in sections 5.1 and 5.2 were based on the processing the same video recording from the experiment. For more accurate results a third method was introduced working with the solutions coming out from *Out1*, *Out2* and *Out3* outputs. These samples were stored inside eppendorf tubes and then dispersed on the surface of the Bürker chamber. After, a thin glass plate was placed on the sample to thin the layer of liquid and make the microbeads visible. The chamber has thin notches forming a grid which are guidelines for the measurements (the particles are only counted if they are inside the grid). This way with each measurement the same volume of fluid gets examined.

6. Results

The devices were compared based on their particle focusing abilities. The performance is measured by number of particles leaving the device on the outlets. The performance is assessed better if more particles exit the system on *Out2* and less on *Out1* and *Out3* (figure 6.). This way the devices are comparable and the best performing one can be selected and further modified.

It is important to highlight the fact that all the measurements were executed once, consequently the results are not as precise as the average of more experiments. These measurements can only be called accurate if at least two or more tests were performed and their average results were calculated. The outcomes of the measurements presented below can only be discussed as approximate results in the perspective of the above statements.

The devices were measured in two sections. The first section (section 6.1) was a different channel width comparison based on focusing ability, the second one (section 6.2) examined the length of the parallel segments as the main manipulator of the focusing performance.

Figure 6: Naming of the different outlets of the device: The outlets of the microfluidic

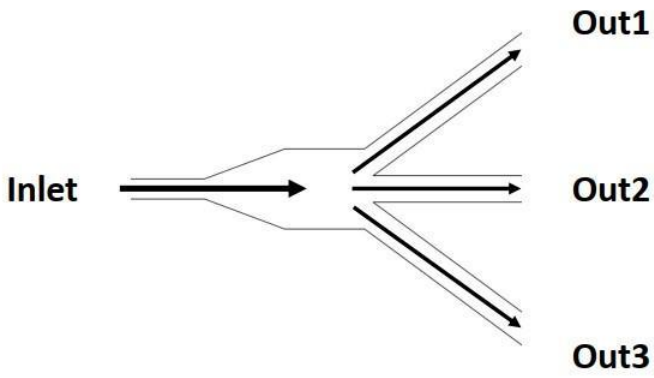

chip in this article are named and referenced based on this figure.

Source: Own work, 2022

6.1. Comparison of channel width modified devices

As a first approach, the effect the channel width modification has on the particle focusing ability of the device was examined. Three different chip version was designed and tested to evaluate the results, each having different channel width (100, 150 and 200 μm) as shown on figure 7. The results were evaluated using the techniques discussed in section 5.

Figure 7: The naming of the measurements: The flow rate is determined by the channel width as shown on the top right corner. The labeling of the different measurements consists of three parameters: the channel width (µm), the diameter (µm) of the microbeads used in the experimental solution and the flow rate (ml/h). For example, a measurement made with a device having **150**µm channel width and a solution having **5**µm diameter microbeads (and having a flow rate of 20 ml/h which is determined by the channel width) is referenced as "measurement 150/5/20".

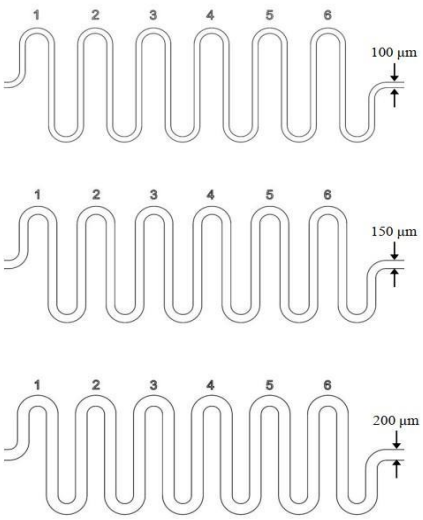

Flow rate is determined by the channel width

Channel width (μm)	Flow rate (ml/h)
100	8
150	20
200	25

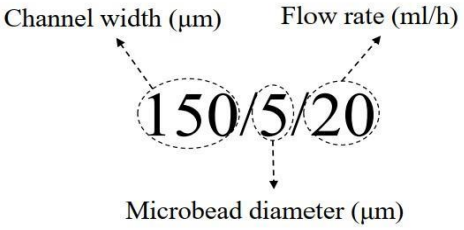

Source: Own work, 2022

All devices were tested using 5 and 10 μm microbeads. At first, the 100 μm channel was examined using 2 μm beads, but the focusing ability was far behind the 5 and 10 μm beads therefore the *100/2/8* measurement (shown on figure 8) was declared unsuccessful and the *150/2/20* and *200/2/25* experiments were not been executed. Measurement *100/2/8* is also used for reference to the others as it gives a baseline with which the other experiments can be compared. The comparisons of the experiments using different sized microbeads on the same microfluidic devices are shown on figures 15. (for measurements *100/2/8, 100/5/8* and *100/10/8*), 16. (for measurements *150/5/20* and *150/10/20*) and 17. (for measurements *200/5/25* and *200/10/25*). These figures can also be compared to see the difference between different channel widths. The comparison shows that the smaller the channel width gets the better the focusing ability becomes.

Figure 8: Measurement 100/2/8: As the results show the device cannot focus the particles to the middle outlet. This measurement is best treated as a reference for the other, better preforming ones.

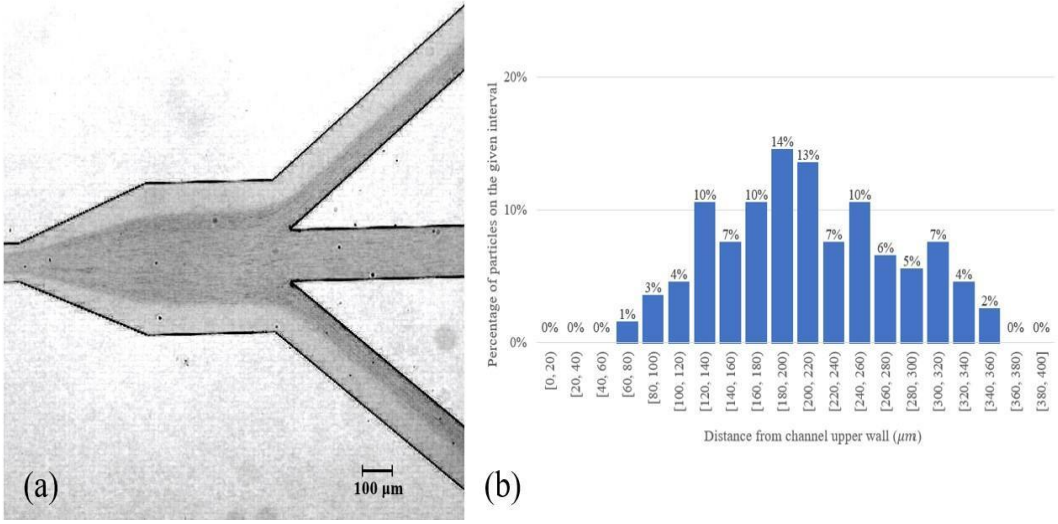

Source: Own work, 2022

6.1.1. Image processing results

The measurements were treated using image processing method. The following measurements were executed: *100/5/8* (figure 9), *100/10/8* (figure 10), *150/5/20* (figure 11), *150/10/20* (figure 12), *200/5/25* (figure 13), *200/10/25* (figure 14). The results show that the smaller the channel width the better the results get, as well as the bigger the diameter of the microbeads get, the focusing ability improves.

Figure 9: Measurement 100/5/8: Timelapse imaging (section 5.1) and image processing (section 5.2) were used for evaluating the results of the experiments. On figure (a) the timelapse image is shown while figure (b) presents the particle distribution in the channel. This experiment proved better focusing ability than measurement 100/2/8.

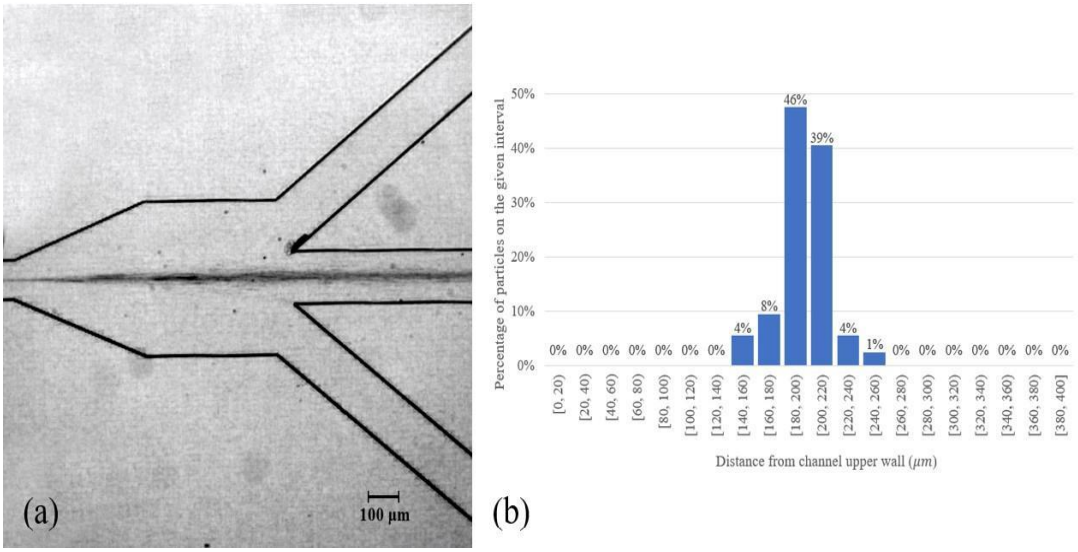

Source: Own work, 2022

Figure 10: Measurement 100/10/8: Timelapse imaging (section 5.1) and image processing (section 5.2) were used for evaluating the results of the experiments. On figure (a) the timelapse image is shown while figure (b) presents the particle distribution in the channel. This experiment proved better focusing ability than measurements 100/2/8 and 100/5/8.

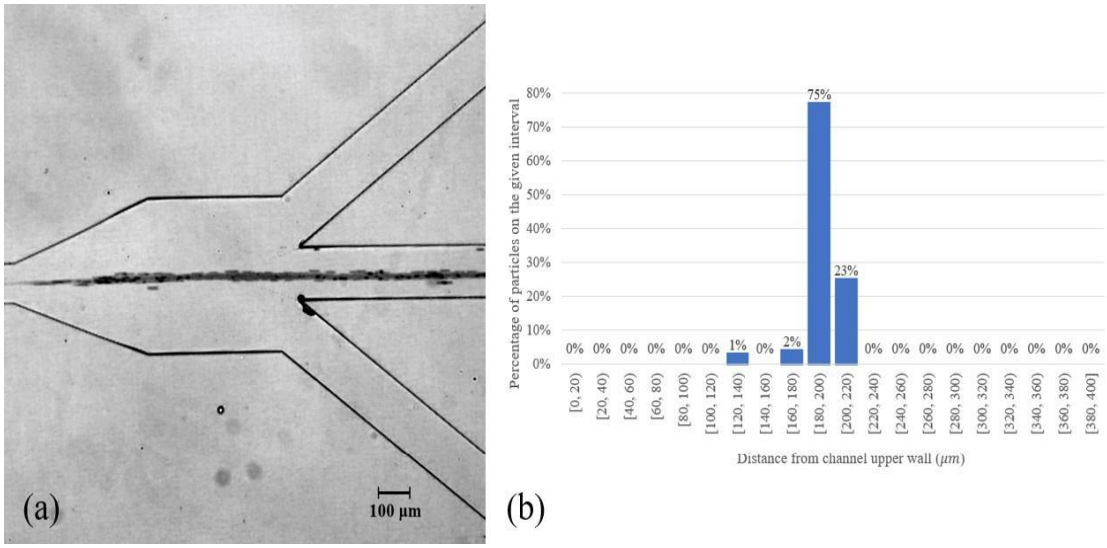

Source: Own work, 2022

Figure 11: Measurement 150/5/20: Timelapse imaging (section 5.1) and image processing (section 5.2) were used for evaluating the results of the experiments. On figure (a) the timelapse image is shown while figure (b) presents the particle distribution in the channel. This experiment proved better focusing ability than measurement 100/2/8 but the particles were scattering a bit more than in measurement 100/5/8.

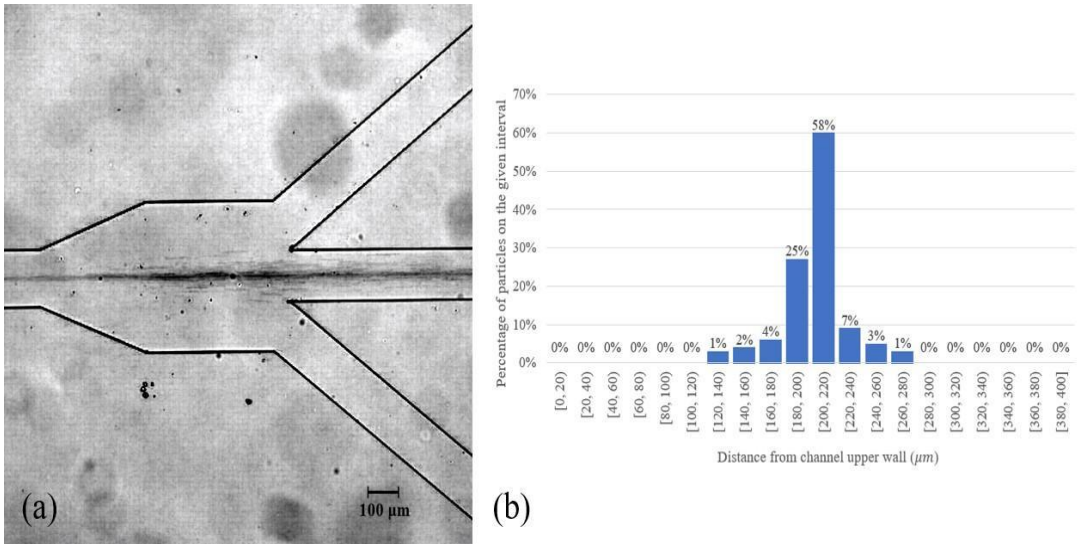

Source: Own work, 2022

Figure 12: Measurement 150/10/20: Timelapse imaging (section 5.1) and image processing (section 5.2) were used for evaluating the results of the experiments. On figure (a) the timelapse image is shown while figure (b) presents the particle distribution in the channel. This experiment proved better focusing ability than measurements 150/5/20 but it was weaker than measurement 100/10/8.

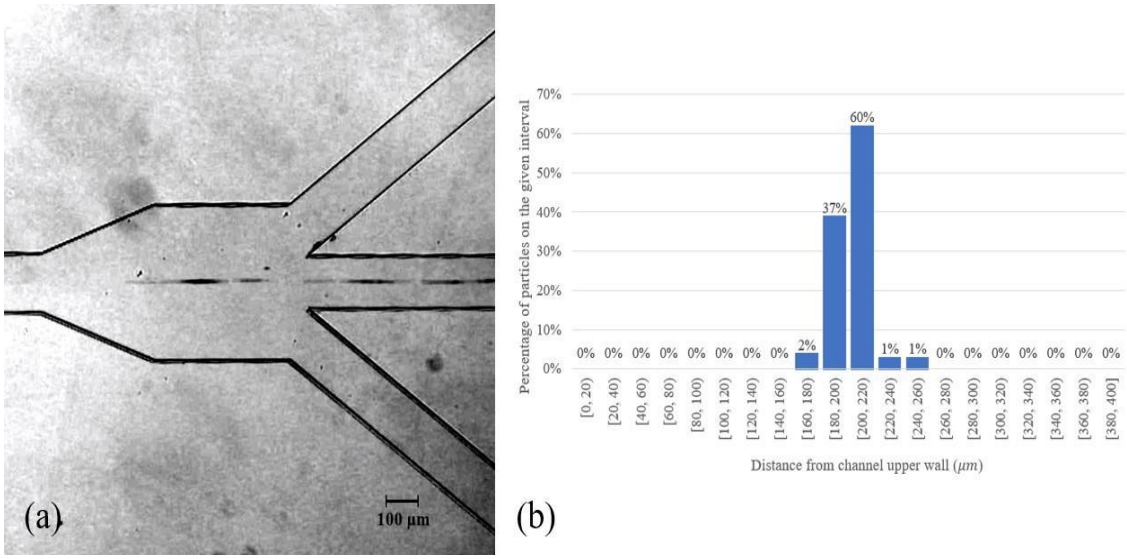

Source: Own work, 2022

Figure 13: Measurement 200/5/25: Timelapse imaging (section 5.1) and image processing (section 5.2) were used for evaluating the results of the experiments. On figure (a) the timelapse image is shown while figure (b) presents the particle distribution in the channel. This experiment proved better focusing ability than measurements 100/2/8 but it was weaker than any previous experiments.

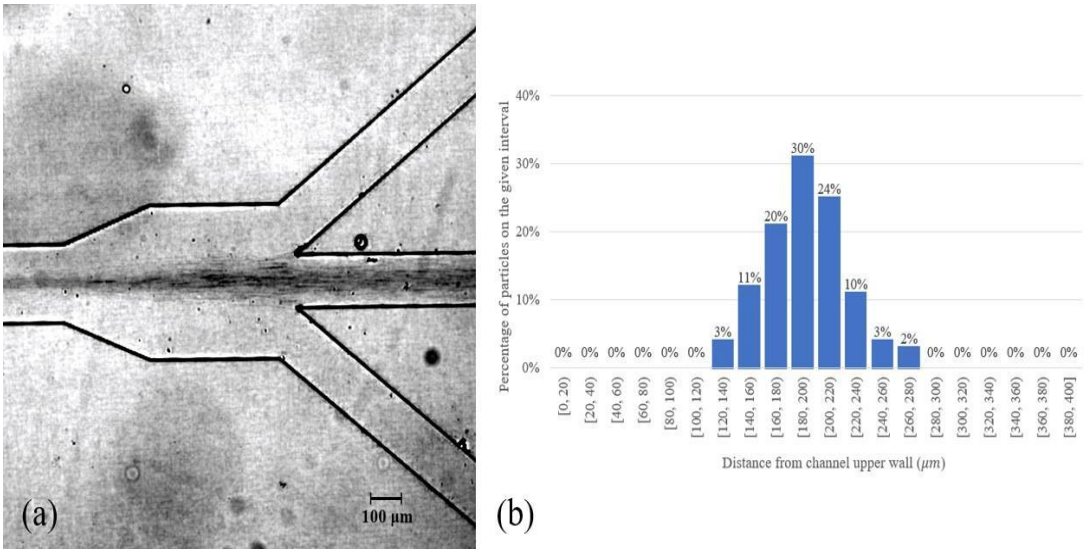

Source: Own work, 2022

Figure 14: Measurement 200/10/25: Timelapse imaging (section 5.1) and image processing (section 5.2) were used for evaluating the results of the experiments. On figure (a) the timelapse image is shown while figure (b) presents the particle distribution in the channel. This experiment proved better focusing ability than measurements 200/5/25 but it was weaker than the previous experiments with the same microbead size.

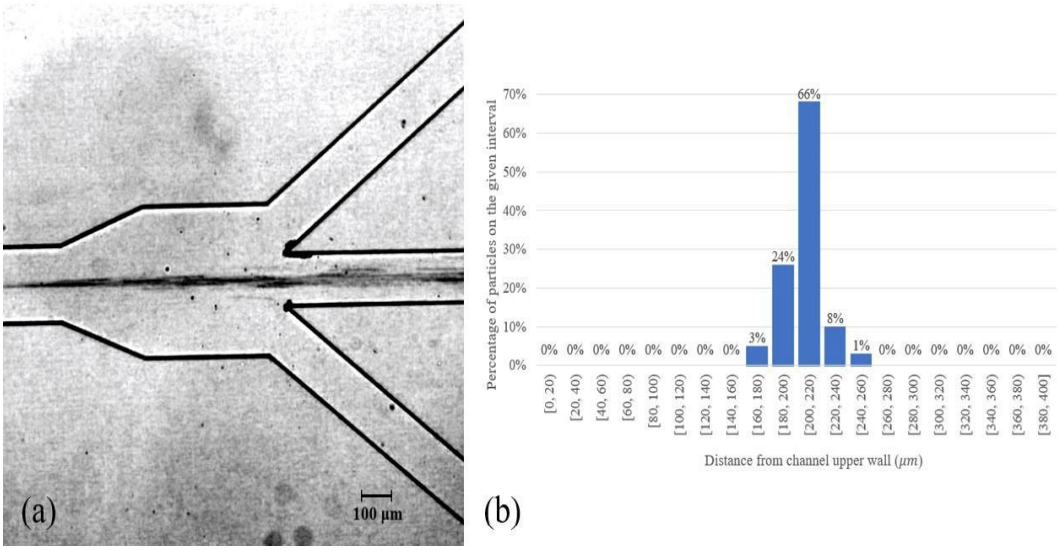

Source: Own work, 2022

Figure 15: Comparison of the measurements executed on the device having 100 µm channel width: The results show that the bigger the microbead diameter gets the better the focusing ability becomes.

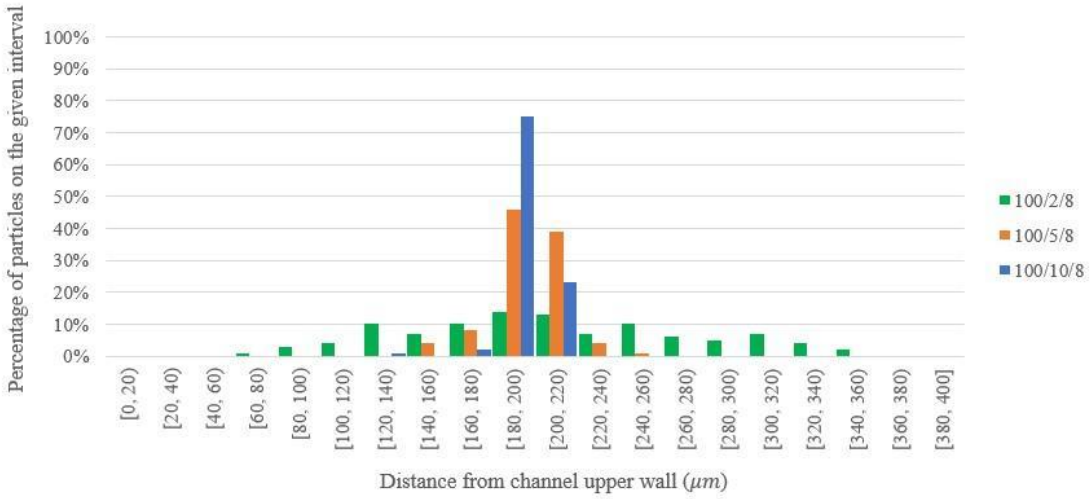

Source: Own work, 2022

Figure 16: Comparison of the measurements executed on the device having 150 µm channel width: The results show that the bigger the microbead diameter gets the better the focusing ability becomes.

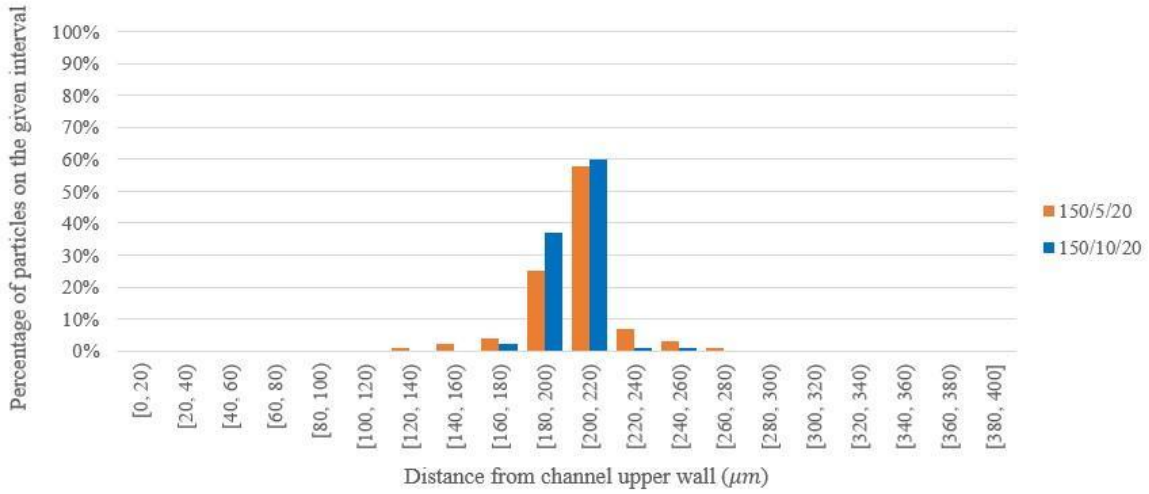

Source: Own work, 2022

Figure 17: Comparison of the measurements executed on the device having 200 µm channel width: The results show that the bigger the microbead diameter gets the better the focusing ability becomes.

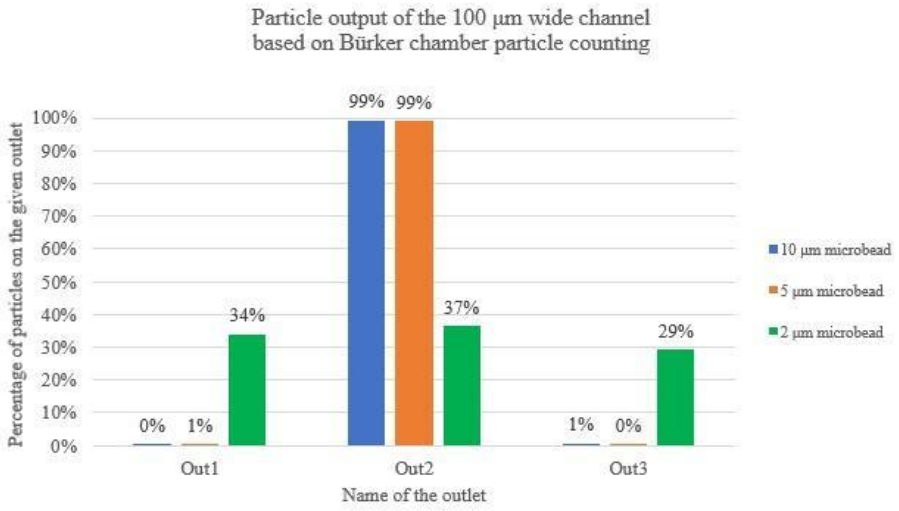

Source: Own work, 2022

6.1.2. Bürker chamber particle counting results

The outputs of the devices were measured using Bürker chamber particle counting as well (section 5.3). These results were compared with the image processing-based measurements for further accuracy. The measurement outcomes are demonstrated on figures

18, 19 and 20. The measurements show that the bigger the microbead size gets the better the focusing ability becomes in the devices.

Figure 18: Bürker chamber particle counting results of the 100 µm wide channel: The results show the percentage of particles exiting the system on the different outlets.

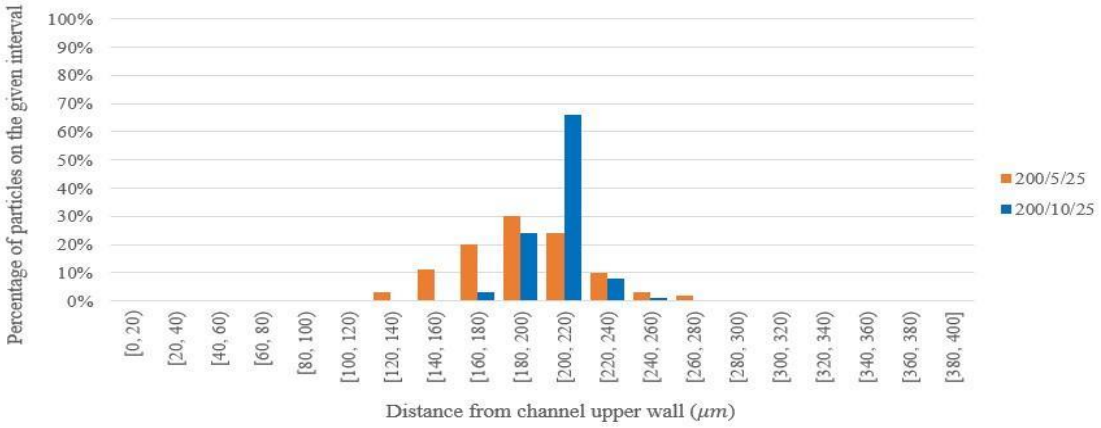

Source: Own work, 2022

Figure 19: Bürker chamber particle counting results of the 150 µm wide channel: The results show the percentage of particles exiting the system on the different outlets.

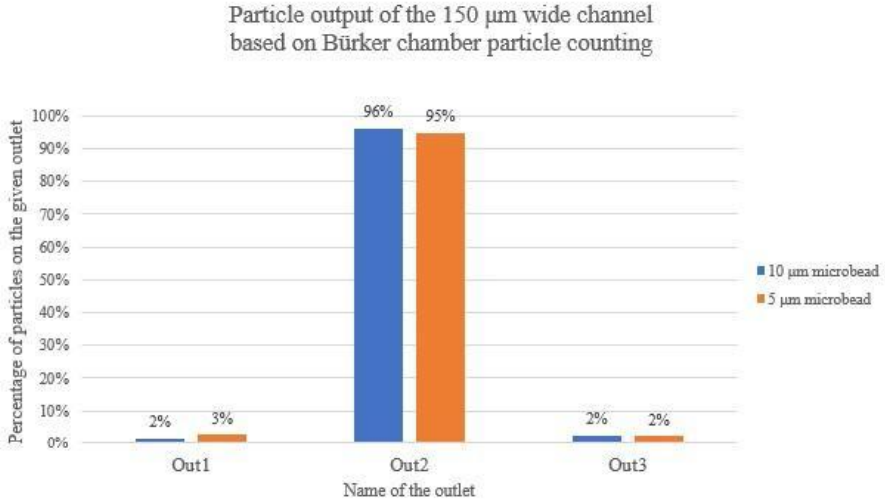

Source: own work, 2022

Figure 20: Bürker chamber particle counting results of the 200 µm wide channel: The results show the percentage of particles exiting the system on the different outlets.

Source: Own work, 2022

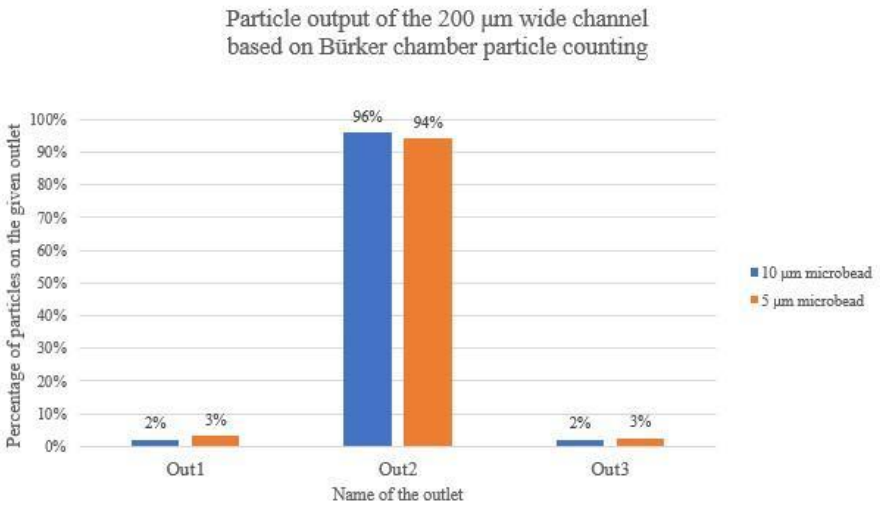

6.2. Comparison of parallel segment length modified devices

After measuring the difference, the varying channel width made on focusing, another series of experiments were planned where the length of the parallel segments (in the serpentine section) was modified (as shown on figure 21). Measurement 100/5/8 (figure 9) was used in this comparison as well as it has 1.5 mm parallel segment length therefore only the experiments with 0.5, 1.0- and 2.0-mm parallel segment lengths were had to be performed. These experiments were named as shown on figure 21., namely measurements *100/5/8/0.5*, *100/5/8/1.0*, *100/5/8/1.5* and *100/5/8/2.0*.

The processing methods of the measurements are the same as in section 6.1, this way the results are comparable with each other.

Figure 21: The modifications of the length of the parallel segments and the nomenclature of the measurements: For better comparability the devices were having the same (100 µm) channel width and were tested using 5 µm microbeads on 8 ml/h flow rate.

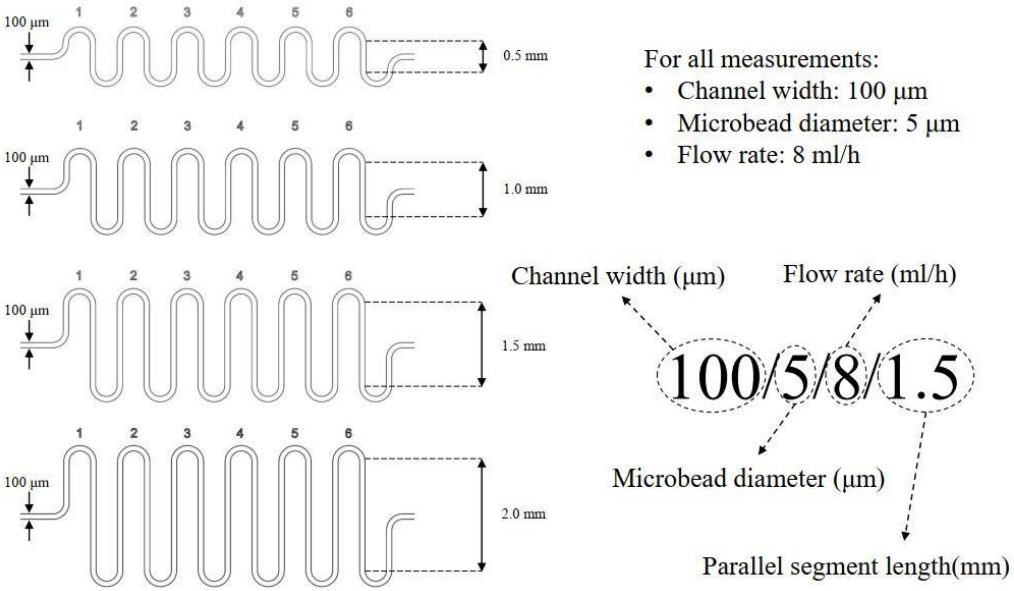

Source: Own work, 2022

6.2.1. Image processing results

The results of the experiments executed are shown on figures 22. (measurement *100/5/8/0.5*), 23. (measurement *100/5/8/1.0*), 24. (measurement *100/5/8/1.5*) and 25. (measurement *100/5/8/2.0*). These show that with increasing the length the focusing ability also improves.

6.2.2. Bürker chamber particle counting results

The device outputs were measured using Bürker chamber particle counting. The results are shown on figure 26. The measurements show that the bigger the microbead size gets the better the focusing ability becomes in the devices.

Figure 22: Measurement 100/5/8/0.5: Timelapse imaging (section 5.1) and image processing (section 5.2) were used for evaluating the results of the experiments. On figure (a) the timelapse image is shown while figure (b) presents the particle distribution in the channel. Based on the results, smaller parallel segment lengths do not give better results.

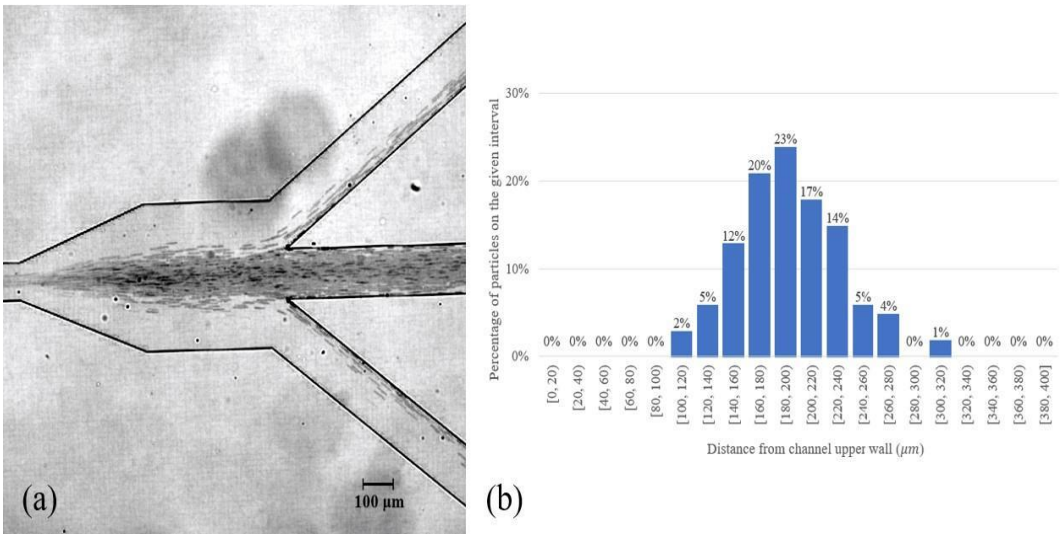

Source: Own work, 2022

Figure 23: Measurement 100/5/8/1.0: Timelapse imaging (section 5.1) and image processing (section 5.2) were used for evaluating the results of the experiments. On figure (a) the timelapse image is shown while figure (b) presents the particle distribution in the channel. The results are better than in measurement 100/5/8/0.5 (figure 22.) but still behind the results of the measurements having 1.5 mm and 2.0 mm parallel segment lengths.

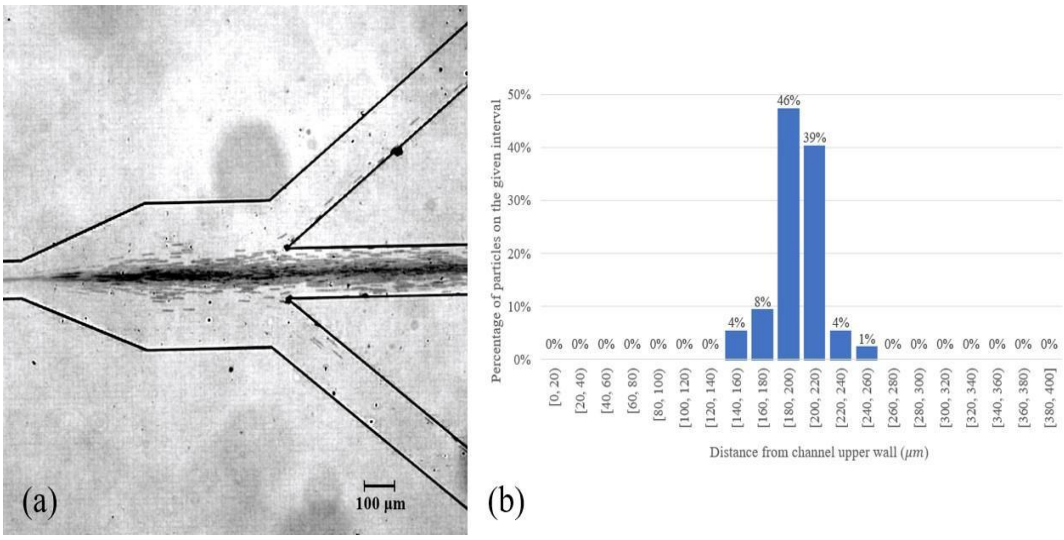

Source: Own work, 2022

Figure 24: Measurement 100/5/8/1.5**:** Timelapse imaging (section 5.1) and image processing (section 5.2) were used for evaluating the results of the experiments. On figure (a) the timelapse image is shown while figure (b) presents the particle distribution in the channel. This is the 100/5/8 measurement seen on figure 9. It has better performance than measurements 100/5/8/0.5 and 100/5/8/1.0.

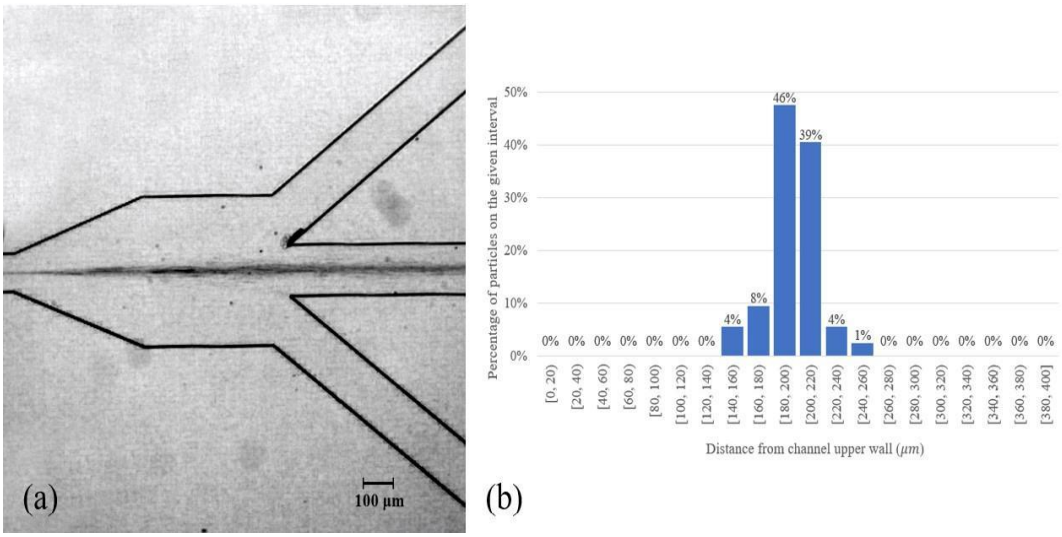

Source: Own work, 2022

Figure 25: Measurement 100/5/8/2.0: Timelapse imaging (section 5.1) and image processing (section 5.2) were used for evaluating the results of the experiments. On figure (a) the timelapse image is shown while figure (b) presents the particle distribution in the channel. By having the best performance from the measurements having modified parallel segment length this experiment proves that the longer the parallel segment gets the better the focusing results become.

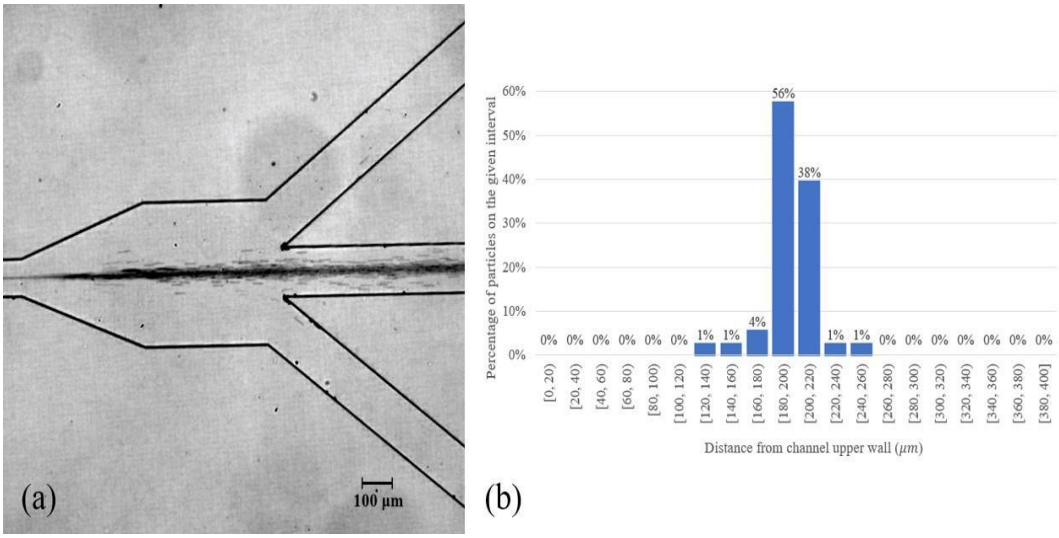

Source: Own work, 2022

Figure 26: Bürker chamber particle counting results of the parallel segment length modified devices: The results show the significant improvement in terms of focusing ability as the parallel segment length gets longer.

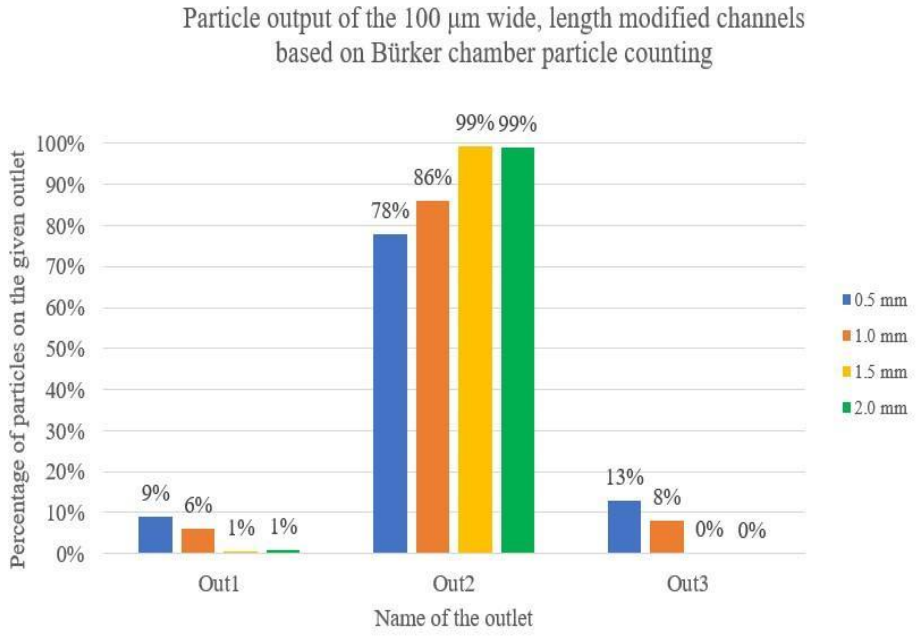

Source: Own work, 2022

7. Conclusion

The experiments discussed in section 6 show that the channel width, the size of the microbeads and also the length of the parallel sections in the serpentine region all are having a huge influence on the focusing performance of the device.

The results show that the narrowing of the channel makes the overall focusing ability better. The size of the microbeads also influences the performance in a way that the bigger their diameter gets the better the performance will be (at least until 10 μm beads as they were the biggest particles tested during the experiments). Lastly, as the length of the parallel segments gets bigger the focusing ability improves, this may be because the overall length of the device increases, and the particles have longer distance available to drift to the middle of the channel in the serpentine region.

Summing up the results, the 100 μm wide channel with 1.5 mm long parallel segments preformed the best (and it was measured using 10 μm beads). Theoretically this device can be further improved if measured with a modified parallel segment length of 2.0 mm because the results show that longer serpentine region lengths give better focusing results.

Further measurements can be conducted in the future to find if there are other parameters influencing the focusing ability of the device beside those discussed in this report.

8. Acknowledgement

I want to thank to my supervisor, Dr. András József Laki for supporting me during the whole process of these experiments and during the essay compositing. I also want to thank for the Biomicrofluidic Laboratory for supporting my work especially for Mária Laki who helped me to execute the measurements and was answering my questions during the work.

References

Akther, F., Yakob, S. B., Nguyen, N.-T., & Ta, H. T. (2020). Surface Modification Techniques for Endothelial Cell Seeding in PDMS Microfluidic Devices. *Biosensors*, *10*(11), 182. doi:10.3390/bios10110182

CKX53 | Compact Cell Culture Microscope | Olympus LS. (n.d.). Retrieved 18 May 2022, from https://www.olympus-lifescience.com/en/microscopes/inverted/ckx53/

Martel, J. M., & Toner, M. (2014). Inertial Focusing in Microfluidics. *Annual Review of Biomedical Engineering*, *16*(1), 371–396. doi:10.1146/annurev-bioeng-121813-120704

Narayanamurthy, V., E. Jeroish, Z., S. Bhuvaneshwari, K., Bayat, P., Premkumar, R., Samsuri, F., & M. Yusoff, M. (2020). Advances in passively driven microfluidics and lab-on-chip devices: a comprehensive literature review and patent analysis. *RSC Advances*, *10*(20), 11652–11680. doi:10.1039/D0RA00263A

Nivedita, N., Ligrani, P., & Papautsky, I. (2017). Dean Flow Dynamics in Low-Aspect Ratio Spiral Microchannels. *Scientific Reports*, *7*(1), 44072. doi:10.1038/srep44072

Silicon Wafers, Si-Wafers - SIEGERT WAFER GmbH. (n.d.). Retrieved 18 May 2022, from https://www.siegertwafer.com/Silicon_Wafers.html

SU-8 2000 series – Microresist. (n.d.). Retrieved 18 May 2022, from https://www.microresist.de/en/produkt/su-8-2000-series/

SYLGARD™ 184 Silicone Elastomer Kit. (n.d.). Retrieved 18 May 2022, from https://www.dow.com/en-us/pdp.html

Syringe Pump - Advanced Precision Programmable Syringe Pumps - SyringePump.com. (n.d.). Retrieved 18 May 2022, from https://www.syringepump.com/NE-1000.php

UI-3180CP Rev. 2.1. (n.d.). Retrieved 18 May 2022, from https://en.ids-imaging.com/store/ui-3180cp-rev-2-1.html

Xiang, N., Chen, K., Dai, Q., Jiang, D., Sun, D., & Ni, Z. (2015). Inertia-induced focusing dynamics of microparticles throughout a curved microfluidic channel. *Microfluidics and Nanofluidics*, *18*(1), 29–39. doi:10.1007/s10404-014-1395-x

Xiang, N., Ni, Z., & Yi, H. (2018). Concentration-controlled particle focusing in spiral elasto-inertial microfluidic devices. *ELECTROPHORESIS*, *39*(2), 417–424. doi:10.1002/elps.201700150